

# Validating Convex Optimization of Reconfigurable Intelligent Surfaces via Measurements

Hans-Dieter Lang\*, Michel A. Nyffenegger\*, Sven Keller\*, Patrik Stöckli\*,  
Nathan A. Hoffman\*, Heinz Mathis\*, and Xingqi Zhang†

\*OST – Eastern Switzerland University of Applied Sciences, Rapperswil, SG, Switzerland. Email: hansdieter.lang@ost.ch

†School of Electrical and Electronic Engineering, University College Dublin, Dublin, Ireland.

**Abstract**—Reconfigurable Intelligent Surfaces (RISs) can be designed in various ways. A previously proposed semidefinite relaxation-based optimization method for maximizing power transfer efficiency showed promise, but earlier results were only theoretical. This paper evaluates a small RIS at 3.55 GHz, the center of the 5G band “n78”, for practical verification of this method. The presented results not only empirically confirm the desired performance of the optimized RIS, but also affirm the optimality of the resulting reactance values. Additionally, this paper discusses several practical aspects of RIS design and measurement, such as the operation of varactor diodes and time gating to omit the direct line-of-sight (LOS) path.

**Index Terms**—Reconfigurable Intelligent Surface (RIS), Meta-surface, Scattering, Optimization Methods, Loaded Antennas.

## I. INTRODUCTION

### A. Background

Reconfigurable Intelligent Surfaces (RISs) are broadly considered to be pivotal in upcoming wireless communication technologies and networks, including those categorized as “beyond 5G” (B5G) as well as 6G and beyond [1]–[3]. Hence, they have been drawing attention across various research domains including applied electromagnetics, antennas & propagation, and mobile communications [4]–[6].

The underlying principle is to redirect wireless signals, which may otherwise be lost or “spilled”, back into the system, thereby enhancing both coverage and throughput of wireless connections. To ensure these reflections prove advantageous, reflectors must be both adaptable and “intelligent”. This requires them to be controllable in order to optimize overall performance for each respective link. Moreover, such optimization should consider all users and the entire channel and incorporate all additional scatterers in the vicinity.

Ultimately, the employment of RISs strives not only to mitigate the necessity for supplementary base stations, conserving both costs and energy, but also to amplify energy efficiency and fortify overarching sustainability in forthcoming wireless communication systems.

### B. Overview of Related Work

Several RIS design methodologies are explored in the literature, see e.g., [5], [6]. Binary control of RIS elements is a common method that simply switches elements on or off, providing a simple but limited control mechanism. Other

prevalent approaches incorporate impedance boundary considerations or involve typical metasurface design methods, frequently relying on (locally) periodic approximations that also have their limitations [7].

This project adopts reactive loading as in the design of reconfigurable reflectarrays [8]. This enables continuous phase adjustment of the reflected wave, offering enhanced RIS control, without the limitations of binary on/off states. The question is, how the reactances are obtained.

In [9] it was proposed to use an optimization method to maximize power transfer from a transmitter via RIS to a receiver to find the optimum loading reactances. The method is based on a semidefinite relaxation of the otherwise non-convex underlying optimization problem that showed promising results in simulation, however an empirical verification via measurements was amiss. It had only been verified in relatively simple, non-reconfigurable transmit array scenarios [10]. Optimality of the loading reactances was not shown. This paper aims to fill that gap, thereby confirming the validity and practicality of the proposed method.

### C. Objectives & Outline

This paper delivers empirical validation via measurements of an optimization framework previously proposed for RIS, which to this point had only been explored in simulation. To facilitate this, an RIS design is described and a comprehensive measurement setup is developed. Several measurement results will affirm the validity and applicability of the aforementioned optimization method. Furthermore, various practical facets of both the RIS design and the measurement approaches are explored and discussed.

In the following, Section II delves into the specific wireless scenario under consideration, while Section III explores the practical implementation of the reconfigurable reflectarray, accompanied by a discussion of its inherent limitations. Finally, Section IV presents measurement results, serving to validate the proposed approach.

## II. PRELIMINARIES

### A. Wireless Channel Setup

The wireless communication scenario under consideration is shown in Fig. 1: A flat RIS consisting of several independently tunable antenna elements establishes a non-line-of-sight

(NLOS) wireless channel from the transmitter antenna to the receiver antenna. The former is located at an incident angle  $\beta$  w.r.t. the normal of the surface, whereas the latter is placed at the reflection angle  $\alpha$ . The line-of-sight (LOS) path between the transmitter and receiver is assumed to be obstructed, i.e., no LOS connection exists. This is not required, but a very practical scenario that makes the RIS more significant.

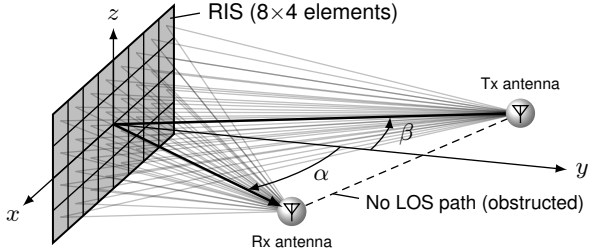


Figure 1. Geometric illustration of the setup: The RIS facilitates an NLOS communication channel between the transmitter and the receiver antennas, positioned at angles  $\beta$  and  $\alpha$  w.r.t. the surface normal, respectively.

Generally, the transmitter and receiver antennas are located at different distances from the RIS. However, for simplicity and ease of practical verification, herein both are positioned at a constant distance  $d = 2$  m from the RIS center. Moreover, the measurement setup confines considerations to incident and reflection angles within the  $\pm 90^\circ$  range off broadside from the RIS. However, the methodology is not exclusive to reflecting RISs; it could also be applied to transmitting RISs or simultaneously transmitting and reflecting STAR-RISs [11].

### B. Review of Convex Optimization of RIS-based Systems

The methodology proposed in [9] treats the entire wireless link from the transmitter antenna via RIS to the receiver antenna as an  $(N + 2) \times (N + 2)$  impedance matrix  $\mathbf{Z}$ , where  $N$  represents the number of antennas (ports) of the RIS that contain tunable elements. The unloaded impedance matrix of the entire system is obtained via simulation, e.g., in ANSYS HFSS with FEBI boundaries to cut down simulation time. The LOS path is omitted by zeroing the respective matrix entries.

Maximizing the power at the receiver antenna port, while holding the transmit power constant and enforcing passivity at all RIS antenna ports, yields optimal reactance values for these ports. Hence, when the RIS antenna ports are then terminated with these optimal reactances, the optimal operation conditions are attained and the RIS provides the maximum performance enhancement of the wireless channel in that configuration.

As outlined in [9], this optimization method employs a convex semidefinite relaxation of the otherwise non-convex and thus "unsolvable" problem. Although there is no assurance that this relaxation is tight—meaning it necessarily leads to the true global optimum of the actual problem—a straightforward test can confirm its validity. As experienced in the original paper, the optimization was successful in all tested cases.

## III. PRACTICAL IMPLEMENTATION

### A. Reflectarray Design

The RIS under consideration follows the design from [9]. However, for simplicity it only consists of two rows of 7 flat dipoles, i.e., a total of 14 tunable elements, as shown in Fig. 2. The frequency under consideration is 3.55 GHz, the center of the 5G band "n78". The antenna elements are spaced 40 mm apart from one another and 1.6 mm-thick copper-backed FR4 is used as dielectric substrate.

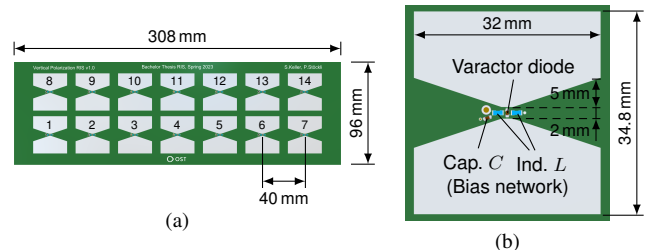


Figure 2. The full RIS (a) and its unit cell (b) with the varactor diode and bias network consisting of two inductors and a capacitor shown.

### B. Varactor Diodes

Reverse-biased varactor diodes are used as tunable capacitors. While this is common for applications below optical and mmWave frequency ranges, also PIN diode designs can be found in recent literature, see for example [12], [13]. Beyond that, MEMS and liquid crystals have also been investigated for tunability [14]. Note that the method used herein is not limited to varactor diodes; any tunable element that can be operated to provide a particular reactance value is suitable.

The SMV2201-040LF varactor diode from Skyworks [15] was selected for this project due to its capability to achieve one of the smallest capacitances available, ranging from 0.23 to 2.1 pF as shown in Fig. 3, covering most of the desired values. The datasheet indicates that different devices can vary by 50% for very small capacitances and 10% for larger ones, which may impact the accuracy of the validation in practice.

1) *Varactor Diode Model*: In general, for reliable results, the equivalent RLC circuit of the varactor diodes must be extracted from measurements [16]. However, in this case, the limited values available in the datasheet were used to find a low-order polynomial for the required voltage  $v$  to obtain a

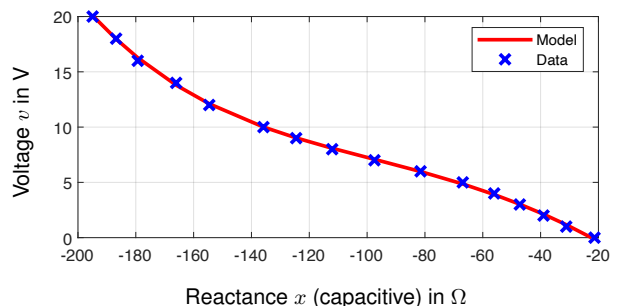


Figure 3. The Skyworks SMV2201-040LF varactor diode.

desired reactance value  $x$ . As shown in Fig. 3, the following polynomial approximation is used for the SMV2201-040LF:

$$v(x) = a + bx + cx^2 + dx^3 + ex^4 \quad (1)$$

with the coefficients  $a = -3.55 \text{ V}$ ,  $b = -1.77 \times 10^{-1} \frac{\text{V}}{\Omega}$ ,  $c = -8.28 \times 10^{-4} \frac{\text{V}}{\Omega^2}$ ,  $d = 8.5 \times 10^{-8} \frac{\text{V}}{\Omega^3}$ , and  $e = 1.47 \times 10^{-8} \frac{\text{V}}{\Omega^4}$ .

The loss resistance of the diode is about  $5.4 \Omega$  according to the datasheet [15]. This was confirmed by measurement and cannot be neglected when using it for large capacitance values.

2) *Bias Network*: The bias network, designed for the varactor diodes, incorporates two inductors of  $L = 33 \text{ nH} \pm 2\%$  (Murata LQW18AN33NG00D) and a capacitor, with a capacitance of  $C = 3.9 \text{ pF} \pm 0.1 \text{ pF}$  (Johanson 500R07S39RBV4S). Both components were strategically selected to ensure that their self-resonance frequencies align closely with the operational frequency. As shown in Fig. 2(b), the layout was designed to maintain symmetry as much as possible.

3) *Limited Range of Values*: The optimization process may potentially yield either inductive or capacitive reactance values that are unattainable with the varactor diodes. In such instances, the corresponding ports are terminated with the nearest realizable suboptimal values—specifically, approximately  $2.1 \text{ pF}$  (equivalent to a reactance  $x \approx -20 \Omega$ ) at  $0 \text{ V}$  or  $0.23 \text{ pF}$  ( $x \approx -200 \Omega$ ) at  $20 \text{ V}$ . The remaining impedance matrix could be re-optimized utilizing the previously mentioned optimization framework or the optimization could be adapted to constrain the reactive loads. However, this is beyond the scope of this paper.

### C. RIS Controller

An RIS controller board was developed to supply the required voltages to the varactor diodes. Anticipating the needs of larger designs in future projects, the DAC60096 by Texas Instruments was chosen. Because its output voltage is limited to  $10.5 \text{ V}$ , but  $20 \text{ V}$  are required to obtain sufficiently low capacitance values from the varactor diodes, it is utilized in conjunction with an amplifier stage, depicted in Fig. 4.

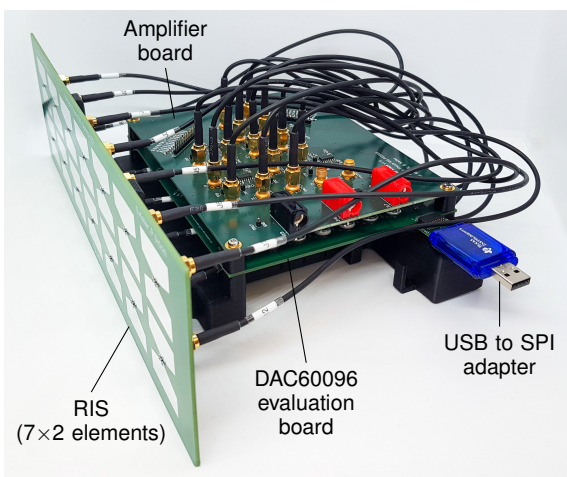


Figure 4. Photo of the fully assembled RIS featuring the controller, composed of the DAC and amplifier boards, mounted on its rear side.

The NCS21914 operational amplifiers by ON Semiconductors were selected for this stage, due to their ability to deliver satisfactory gain and stability while preserving low-power consumption. Additionally, they provide a high input impedance and exhibit rail-to-rail capabilities when deployed with an asymmetric power supply.

## IV. MEASUREMENTS

### A. Measurement Setup

Measuring RISs is inherently challenging, because it often requires distances that exceed the capabilities of smaller anechoic chambers—a scenario encountered in this study as well. To address this, three movable absorber walls were constructed and a dedicated measurement setup was developed, as illustrated in Fig. 5. It features two adjustable arms anchored on a central pivot point where their angles are measured by Amphenol Piher angle sensors (PST-360GB1A-C0000-ERA-05K). The arms are independently moved to desired angles by two  $24 \text{ V}$  DC motors, all controlled by a Raspberry Pi 4 (“Angle controller”) connected to a PC over Ethernet.

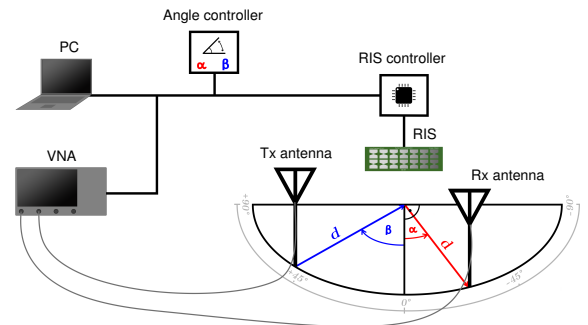


Figure 5. The RIS measurement setup: The two movable arms and the RIS are operated via a PC, which also collates measurement data from the VNA.

Since the received signal of interest is of very low power, reflections from the environment can notably distort the measurement results through interference. Therefore, two QRH11 quad ridged horn antennas by RFspin are used as transmitter and receiver antennas. They provide about  $11 \text{ dBi}$  gain at the frequency of interest and allow for all polarizations to be measured simultaneously, which is not required here, but useful for future considerations. These antennas are mounted on the arms and consistently point to the center of the RIS.

This setup has demonstrated significant utility and versatility. However, it presents the following notable limitations:

- *Reflections from the Environment*: In the measurement setup shown in Fig. 6, effectively eliminating all environmental reflections proves to be a significant challenge. Additional absorbers are placed in the room, particularly on the floor and on the ceiling, to mitigate reflections experienced from those locations. The use of time gating, described in the next subsection, helps further.
- *Far-Field Condition*: At a distance of  $2 \text{ m}$ , the transmitter and receiver antennas are situated approximately at the threshold of the RIS’s far field. Moreover, at small angles



Figure 6. Photo of the measurement setup, featuring two movable antenna arms, a VNA, and the mounted RIS, surrounded by numerous absorbers.

$|\alpha + \beta| \leq 15^\circ$ , the two quad ridge antennas are within their respective near fields. However, such small angles are not possible with the setup anyway. These conditions may impact the measurements, but since the direct path is omitted, the influence is expected to be negligible.

- *Measurement Angle Uncertainty:* The angle controller within the measurement setup exhibits an absolute angle error of  $\pm 1^\circ$ , introducing a potentially non-negligible factor of uncertainty in the reproducibility of measurement results. Moreover, even minor deviations in the antenna angle can yield disparate measurement outcomes.

### B. Time Gating

Time gating is a well-established technique in Vector Network Analyzer (VNA) measurements. For antenna measurements, it is frequently utilized to mitigate imperfections arising from environmental reflections [17]–[19], by applying a filter that basically omits signals outside a certain time-frame.

In this study, a Hann-type gate (i.e., filtering window) was set to start approximately 1 ns prior to the anticipated reflection off the RIS, with a width of 10 ns. Consequently, this effectively omits the direct line-of-sight (LOS) path and minimizes inaccuracies attributed to other environmental reflections. Fig. 7 shows a typical result. Note that the gate/window width should not be chosen too small; the reflection off the RIS takes considerably longer than from a plane reflector.

### C. Verification Results and Discussion

1) *Maximum Bistatic Radar Cross Section (BRCS):* Similar to [9], the bistatic radar cross section (BRCS) is used as a figure of merit to validate the optimization procedure. Fig. 8 depicts the results for a transmitter incident angles  $\beta = -10^\circ$  (red) and  $\beta = -30^\circ$  (blue), respectively, across various angles  $\alpha$  ranging from  $0^\circ$  or  $5^\circ$  to  $45^\circ$  at the aforementioned distance of 2 m. Notably, there is good agreement between the simulated (dashed) and measured (solid lines) values, despite the challenges and influential factors discussed previously. Additionally, while the measurement setup proved to be quite sturdy, it is observed that even minor misalignment can cause deviations of  $\pm 1$  dB in sensitive areas.

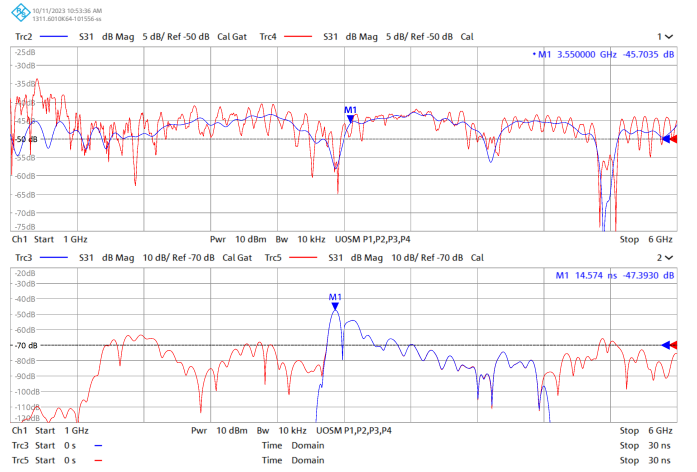


Figure 7. Example of time gating (unmodified screenshot) in both frequency domain (top) and time domain (bottom): The time gate starting at 13 ns omits the direct (LOS) path arriving around 5 ns, while accounting for the indirect path via RIS peaking around 14 ns. This case corresponds to  $\alpha = 20^\circ$  and  $\beta = -10^\circ$  with the original shown in red and the time-gated in blue.

The lighter lines in Fig. 8 provide a comparison of the simulated and measured BRCS of a plane copper reflector with the same dimensions as the array for the two transmitter angles. Given that the simulation utilizes plane-wave excitation, nulls are anticipated to be less pronounced in the measurements. The overall agreement is quite good, apart from minor discrepancies around  $37.5^\circ$ . It is worth noting the distinction between the red and black lines: Even such a small RIS can create a substantial impact at angles sufficiently far from the specular direction.

2) *Optimality of the Obtained Reactances:* Fig. 9 shows three typical behaviors of the capacitor values, obtained by varying one capacitor while maintaining the others at their optimized value. Evidently, the values derived from the optimization algorithm (red dashed lines) are indeed optimal

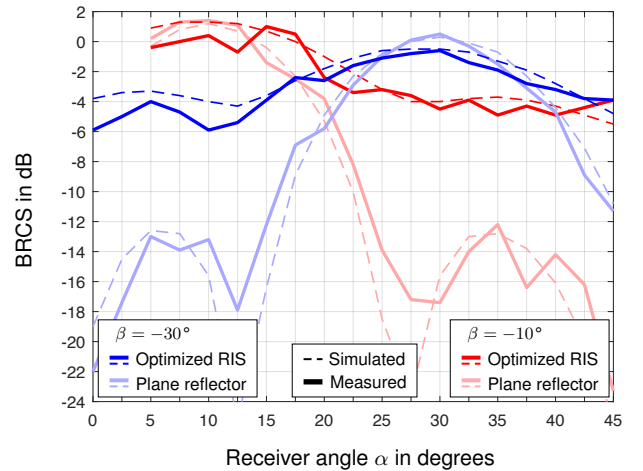


Figure 8. Resulting bistatic radar cross sections (BRCSs) of the optimized RIS and a plane reflector (lighter colors) for the same transmitter angle  $\beta = -10^\circ$  (red) or  $-30^\circ$  (blue) and various receiver angles  $\alpha = 0 \dots 45^\circ$  off broadside (solid: measured, dashed: simulated).

(a) or at least close to optimal (b) and (c). Additionally, it can be observed that the optimum is insensitive to certain capacitances, while exhibiting significant sensitivity to others.

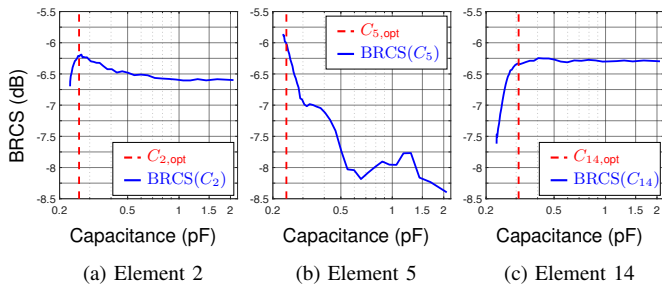


Figure 9. BRCS as a function of different capacitances  $C_n$ , to illustrate typical optimalities and sensitivities of the results obtained from the convex optimization algorithm ( $C_{n,opt}$ , red dashed line), for  $\beta = -10^\circ$  and  $\alpha = 45^\circ$ .

## V. SUMMARY & CONCLUSIONS

Reconfigurable Intelligent Surfaces (RISs), expected to play an important role in future wireless systems, can be designed through various methodologies. Among them is a powerful and versatile optimization framework, treating the RIS as a reflectarray and determining the optimum reactive loads in the antenna elements to maximize the power transferred between transmitter and receiver antennas.

This paper presents a small RIS design to verify a previously proposed optimization method to find the optimum reactive loads in measurements. This task is challenging for various reasons, including the spatial requirements of the measurement setup as well as the limitations and tolerances of the varactor diodes used as variable capacitors. Despite these challenges, results validate the optimization; the obtained capacitance values are optimal or close to it in practice. The use of time gating has proved pivotal, effectively reducing reflections and omitting the line-of-sight path.

In conclusion, the realized RIS not only operates as anticipated, but also serves as a testament to the validity and efficacy of the convex optimization method. It is remarkable that even a small RIS can have a considerable effect at angles far from the specular reflection. Furthermore, the convenient adjustability of the loading reactances allows for precise fine-tuning, helping to bridge any gaps between simulation and real-world outcomes.

## ACKNOWLEDGMENT

This work was carried out as part of the collaborative CHIST-ERA project "Towards Sustainable ICT: Sparse Ubiquitous Networks based on Reconfigurable Intelligent Surfaces (SUNRISE)". The authors of OST are supported by the Swiss National Science Foundation (SNF) with Grant 203784.

## REFERENCES

[1] C. Huang *et al.*, "Holographic MIMO surfaces for 6G wireless networks: Opportunities, challenges, and trends," *IEEE Wireless Communications*, vol. 27, no. 5, pp. 118–125, 2020. doi: 10.1109/MWC.001.1900534

[2] W. Saad, M. Bennis, and M. Chen, "A vision of 6G wireless systems: Applications, trends, technologies, and open research problems," *IEEE Network*, vol. 34, no. 3, pp. 134–142, 2020. doi: 10.1109/MNET.001.1900287

[3] Y. Liu *et al.*, "Robotic communications for 5G and beyond: Challenges and research opportunities," *IEEE Commun. Mag.*, vol. 59, no. 10, pp. 92–98, 2021. doi: 10.1109/MCOM.111.2001118

[4] S. Hu, F. Rusek, and O. Edfors, "Beyond Massive MIMO: The potential of data transmission with large intelligent surfaces," *IEEE Trans. Signal Process.*, vol. 66, no. 10, pp. 2746–2758, 2018. doi: 10.1109/TSP.2018.2816577

[5] C. Huang, A. Zappone, G. C. Alexandropoulos, M. Debbah, and C. Yuen, "Reconfigurable intelligent surfaces for energy efficiency in wireless communication," *IEEE Trans. Wireless Commun.*, vol. 18, no. 8, pp. 4157–4170, 2019. doi: 10.1109/TWC.2019.2922609

[6] M. Di Renzo, A. Zappone, M. Debbah, M.-S. Alouini, C. Yuen, J. de Rosny, and S. Tretyakov, "Smart radio environments empowered by reconfigurable intelligent surfaces: How it works, state of research, and the road ahead," *IEEE J. Sel. Areas Commun.*, vol. 38, no. 11, pp. 2450–2525, 2020. doi: 10.1109/JSAC.2020.3007211

[7] Y. Li, X. Ma, G. Ptitcyn, and S. Tretyakov, "Perfect control of reflection using aperiodic arrays," in *2023 17th European Conference on Antennas and Propagation (EuCAP)*, 2023, pp. 1–3. doi: 10.23919/EuCAP57121.2023.10133273

[8] S. V. Hum and J. Perruisseau-Carrier, "Reconfigurable reflectarrays and array lenses for dynamic antenna beam control: A review," *IEEE Trans. Antennas Propag.*, vol. 62, no. 1, pp. 183–198, 2014. doi: 10.1109/TAP.2013.2287296

[9] H.-D. Lang, M. A. Nyffenegger, H. Mathis, and X. Zhang, "Investigating sparse reconfigurable intelligent surfaces (SRIS) via maximum power transfer efficiency method based on convex relaxation," in *2023 17th European Conference on Antennas and Propagation (EuCAP)*, 2023, pp. 1–5. doi: 10.23919/EuCAP57121.2023.10133402

[10] M. A. Nyffenegger, C. D. Sarris, and H.-D. Lang, "Constrained semidefinite optimization of reactively loaded antenna arrays: Verification and tolerances," in *2021 IEEE International Symposium on Antennas and Propagation and USNC-URSI Radio Science Meeting (APS/URSI)*, 2021, pp. 1645–1646. doi: 10.1109/APS/URSI47566.2021.9704694

[11] Y. Liu *et al.*, "STAR: Simultaneous transmission and reflection for 360° coverage by intelligent surfaces," *IEEE Wireless Communications*, vol. 28, no. 6, pp. 102–109, 2021. doi: 10.1109/MWC.001.2100191

[12] S. Gharbieh, R. D'Errico, and A. Clemente, "Reconfigurable intelligent surface design using PIN diodes via rotation technique - proof of concept," in *2023 17th European Conference on Antennas and Propagation (EuCAP)*, 2023, pp. 1–4. doi: 10.23919/EuCAP57121.2023.10133091

[13] J. H. Oh, J. Jeong, Y. Park, and S.-H. Wi, "A 29 GHz dual-polarized reconfigurable intelligent surface with 2-dimensional wide scanning range," in *2023 17th European Conference on Antennas and Propagation (EuCAP)*, 2023, pp. 1–5. doi: 10.23919/EuCAP57121.2023.10133348

[14] B. Rana, S.-S. Cho, and I.-P. Hong, "Review paper on hardware of reconfigurable intelligent surfaces," *IEEE Access*, vol. 11, pp. 29 614–29 634, 2023. doi: 10.1109/ACCESS.2023.3261547

[15] Skyworks, *SMV2201-SMV2205 Series: Surface Mount, 0402 Silicon Hyperabrupt Tuning Varactor Diodes*, May 2012, available: <https://www.skyworksinc.com/en/Products/Diodes/SMV2201-040LF>.

[16] P. Ratajczak, "Design of a dual polarization reconfigurable intelligent surface at 26.0 GHz for 5G applications," in *2023 17th European Conference on Antennas and Propagation (EuCAP)*, 2023, pp. 1–4. doi: 10.23919/EuCAP57121.2023.10133449

[17] J. Williams, H. Delgado, and S. Long, "An antenna pattern measurement technique for eliminating the fields scattered from the edges of a finite ground plane," *IEEE Transactions on Antennas and Propagation*, vol. 38, no. 11, pp. 1815–1822, 1990. doi: 10.1109/8.102744

[18] P. González-Blanco and M. Sierra-Castañer, "Time filtering techniques for echo reduction in antenna measurements," in *2016 10th European Conference on Antennas and Propagation (EuCAP)*, 2016, pp. 1–3. doi: 10.1109/EuCAP.2016.7481235

[19] R. Phumvijit, P. Supanakoon, and S. Promwong, "Measurement scheme of radar cross section with time gating," in *2017 14th International Conference on Electrical Engineering/Electronics, Computer, Telecommunications and Information Technology (ECTI-CON)*, 2017, pp. 822–825. doi: 10.1109/ECTICon.2017.8096365